

Characterization of Dynamic Behavior of Flexure-based Mechanisms for Precision Angular Alignment

Vijay Shilpiekandula and Kamal Youcef-Toumi

Mechatronics Research Laboratory, Department of Mechanical Engineering
Massachusetts Institute of Technology, Cambridge, MA 02139, USA
Email: svijay@mit.edu, youcef@mit.edu

Abstract—Angular alignment is a critical requirement in numerous precision motion control applications. Examples include beam-steering in optical communications and tool-sample alignment in imprint lithography. Flexural mechanisms are being widely used in such applications. The absence of non-linearities, including friction and backlash, makes flexural components ideal for achieving atomic-scale resolution. Closed-loop control implementations of flexural angle alignment mechanisms have been attempted in the literature in various cases. Performance limitations in closed-loop control implementations have been characterized traditionally considering effects of actuators, sensors, and control algorithms used. However, a critical limiting factor is imposed by the open-loop response of the plant, i.e. the natural frequencies of the flexural mechanism itself. In this paper, we assemble models for characterizing the dynamic behavior of flexural mechanisms for angular alignment. The performance trade-offs in terms of range, load-capacity, and control bandwidth are highlighted. A state-space formulation is proposed for mapping design performance variables, such as vertical deflection or angular acceleration. The effects on dynamic performance imposed by asymmetry resulting from manufacturing errors are studied.

I. INTRODUCTION

Angular alignment is critical to an emerging class of small-scale precision manufacturing and motion control applications. The drive for better performance steers design and control effort into achieving high tolerances and stringent specifications in terms of parameters, such as resolution, range, load-capacity, and bandwidth. Examples of applications needing precision angular alignment include (i) high-bandwidth steering of mirrors in telecommunication applications [1], (ii) tool-sample alignment in stamping applications such as imprint lithography [2], [3] and micro-contact printing [4], and (iii) alignment of optically flat surfaces brought in close proximity to characterize fields and forces on small-scales, such as the Casimir force [5].

A widely used set of designs for precision applications described above involve compliant mechanisms based on slender beam modules, also referred to as flexures [6]. The advantages flexures offer are mainly smooth elastic motion without non-linearities such as friction or backlash [7]. Flexure-based mechanisms such as the diaphragm flexure involve the payload suspended on a radial or tangential arrangement of flexural beams. Various forms of such flexures have appeared over the past few decades for angle alignment and guidance applications [4], [8]. Analysis of the statics and dynamics of flexure-based mechanisms have been extensively studied [7], [9].

While flexure-based engineering designs have been around for many decades [10], designing them for dynamic performance has sought little attention. Few publications have appeared in this context. The design for dynamical performance of flexures in the context of mechanical advantage is detailed in [11]. A finite-element approach based on Euler-Bernoulli beam bending theory is formulated for analyzing dynamics in [12] and optimizing the design space for precision flexure-based applications in [13].

We build on the work presented in the literature and integrate models that can enhance the accuracy in predicting the dynamics of a given flexure-based design by including the effects of distributed mass and compliance of the flexures covering shear and rotational effects. These effects are shown to dominate for flexures with comparable thickness and length. Further, we use the models to characterize design space parameters such as range, load-capacity, and bandwidth. While most of the current literature in flexure-based designs focuses on static values of performance variables such as angular position, or acceleration, we present a state-space approach for characterizing the bounds on these variables in the frequency domain. This is critical for ensuring that performance requirements are met within the usually large bandwidths of operation, an example application being fast steering of mirrors in telecommunications [1].

The rest of this paper is organized as follows. In Section II we assemble lumped parameter models for a diaphragm flexure design. Section III covers the closed-form characterization of the design space from the dynamic models. A state-space approach is used for characterizing key performance variables in Section IV. The effects of manufacturing errors are studied in this section. Finally, we conclude with a summary of the contributions of the work.

II. DYNAMIC MODELING

Our goal is to capture the out-of-plane behavior, i.e. the vertical translation, pitch, and roll degrees of freedom of diaphragm flexures used in precision angle alignment mechanisms. In this section, we assemble dynamic models for a class of diaphragm flexures — namely, those applying radial constraints on a central rigid mass via flexural beam units. We derive lumped parameter models representing the mass and stiffness of the diaphragm flexure.

A. Modeling Flexural Beam

To model bending of the flexural beam unit, shown in Fig. 2, we use a Timoshenko beam [14] model since a simple

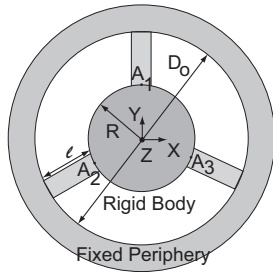


Fig. 1. A diaphragm flexure as a parallel kinematic mechanism with a central rigid mass connected by $n = 3$ flexural beam units to the ground. The dimension $D_0 = 2l + 2R$ is referred in this paper as the footprint of the mechanism. The Z axis is shown pointing out of the page.

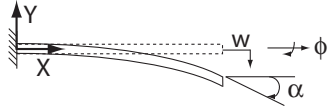


Fig. 2. Schematic diagram showing a flexural beam element with deflection $w(x,t)$, slope $\theta(x,t)$, and twist about the X -axis by an angle $\phi(x,t)$.

Euler-Bernoulli beam model cannot capture the effects of shear and rotational inertia. To model torsion of the flexural element, we use St. Venant's torsion formulation assuming that (i) the effects of restrained warping are negligible and (ii) bending and torsion are decoupled. Further, we assume that the deflections of the flexural beam element are small (an order of magnitude smaller than the beam thickness) and hence, neglect the effects of axial stretching and the resultant stress stiffening along the length of the beam element.

Under the above-mentioned assumptions, the distributed parameter model for the beam is well-documented in the literature [14] as being depicted by a set of partial differential equations in the deflection $w(x,t)$, slope $\theta(x,t)$, and angle of twist $\phi(x,t)$ listed in Section A of the Appendix.

The infinite-dimensional behavior governed by the set of partial differential equations can be approximated to that arising for a one-element model using the method of assumed modes [15]. This method (see [17]) approximates the dynamic response to a finite-series made up of spatially varying mode shape functions (or trial functions) with temporally varying mode amplitudes [16]. Since a one-element model is used for the beam, the distributed properties of the beam are lumped to the node at the guided end of the beam; the fixed node of the beam has no lumped mass or stiffness. Hence, from the three displacements assumed for the guided end of the beam, a three-DOF lumped parameter model can be derived.¹

Under the geometric boundary conditions of (i) one end $x = 0$ of the flexural beam being grounded and (ii) the other end $x = l$ subject to generalized displacements $\mathbf{V}(t) = [w(\ell, t) \ \theta(\ell, t) \ \phi(\ell, t)]^T$, (where $w(\ell, t)$ is the vertical deflection, $\theta(\ell, t)$ the slope, and $\phi(\ell, t)$ is the angle of twist), the

¹A many-element model can be used for each flexural beam to develop higher-order lumped parameter models, if desired. As will be evident from simulations in this paper, assumed modes methods tend to be powerful in that they can converge to the actual plant with relatively lower-order models.

corresponding 3×3 matrices — mass \mathbb{M}_f and stiffness \mathbb{K}_f are as given below:

$$\mathbb{M}_f = \begin{bmatrix} M_1 & M_2 & 0 \\ M_2 & M_3 & 0 \\ 0 & 0 & M_4 \end{bmatrix}; \quad \mathbb{K}_f = \begin{bmatrix} K_1 & K_2 & 0 \\ K_2 & K_3 & 0 \\ 0 & 0 & K_4 \end{bmatrix}$$

where the matrix values depend on material properties and geometry, and are tabulated in Section A. 1 of the Appendix. Formulations for serial kinematic configurations can be developed by altering the choice of geometric boundary conditions [17].

B. Assembling Global Lumped Parameter Model

Here, we formulate the dynamics of parallel kinematic mechanisms that contain a rigid body connected to the ground through a multitude of flexural beam units. We integrate the lumped parameter model for the flexural beam in Section II with rigid body dynamical models using appropriate transformations to obtain the global model [12]. These transformations are chosen to ensure the continuity of nodal displacements at the interface between the rigid body and the flexures.

Consider a parallel kinematic mechanism with a central rigid circular disk centered at the origin and parallel to the horizontal \mathbf{XY} plane of the cartesian \mathbf{XYZ} space, as shown in Fig. 1. In the rest position, the principal axes of the disk \mathbf{X}' , \mathbf{Y}' , and \mathbf{Z}' coincide with the cartesian axes \mathbf{X} , \mathbf{Y} , and \mathbf{Z} , respectively. Let the disk be of radius R , thickness T , mass M_R , and moments of inertia J_{Rxx} and J_{Ryy} about the X and Y axes respectively. A number n of slender beam flexures, each of width W , thickness H , and length ℓ , are in the \mathbf{XY} plane connecting every peripheral point P_i to the ground. The coordinates of P_i in the $\mathbf{X}'\mathbf{Y}'$ plane are $(R\cos\alpha_i, R\sin\alpha_i)$ with angles $\alpha_i \in [0, 2\pi)$ for $i = 1, 2, 3 \dots n$.

Since the beams provide high axial (and hence in-plane \mathbf{XY}) stiffness and low out-of-plane stiffness, we expect that the dominant modes correspond to the out-of-plane motion, namely vertical deflection, pitch, and roll. We hence assume that the out-of-plane motion of the disk is decoupled from the in-plane motion, i.e. the center of the disk always moves only vertically. For small vertical deflection $z(t)$ of the center of mass, and small angular rotations $\theta_x(t)$ and $\theta_y(t)$ about the X and Y axes respectively, the principal plane $\mathbf{X}'\mathbf{Y}'$ of the disk moves out of the \mathbf{XY} plane to the one depicted by

$$\mathbf{Z}_p(t) = \theta_y(t)\mathbf{X} + \theta_x(t)\mathbf{Y} + z(t) \quad (1)$$

For continuity of displacement at each of the nodes P_i , Eq. (1) can be used to show that the end-displacements $\mathbf{V}_i(t)$ of every i^{th} flexure are related to the global generalized (rigid body) displacements $\mathbf{V}_R(t)$ as follows:

$$\mathbf{V}_i(t) = \begin{Bmatrix} w_i(\ell, t) \\ \theta_i(\ell, t) \\ \phi_i(\ell, t) \end{Bmatrix} = \mathfrak{R} \begin{Bmatrix} z(t) \\ \theta_x(t) \\ \theta_y(t) \end{Bmatrix} = \mathfrak{R} \mathbf{V}_R(t)$$

where the transformation matrix $\mathfrak{R} =$

$$\begin{bmatrix} 1 & R\sin\alpha_i & R\cos\alpha_i \\ 0 & -\sin\alpha_i & -\cos\alpha_i \\ 0 & -\cos\alpha_i & -\sin\alpha_i \end{bmatrix}$$

C. Dynamics

By formulating the Lagrangian of the assembly in terms of the rigid body displacements $\mathbf{V}_R(t)$, we develop the lumped mass and stiffness matrices of the overall parallel kinematic mechanism as follows:

$$\mathbb{M} = \sum_{i=1}^n \mathfrak{R}^T \mathbb{M}_{fi} \mathfrak{R} + \mathbb{M}_R; \quad \mathbb{K} = \sum_{i=1}^n \mathfrak{R}^T \mathbb{K}_{fi} \mathfrak{R} \quad (2)$$

where \mathbb{M}_{fi} and \mathbb{K}_{fi} are the lumped mass and stiffness matrices, respectively, of the individual flexure building blocks given in Section II-A, and Tables III and IV; \mathbb{M}_R is the mass matrix of the rigid body and is given by:

$$\begin{bmatrix} M & 0 & 0 \\ 0 & J_{Rxx} & 0 \\ 0 & 0 & J_{Ryy} \end{bmatrix}$$

The equations of motion of the lumped parameter representation, for the free response case, is in the form given below:

$$\mathbb{M}\ddot{\mathbf{V}}_R + \mathbb{B}\dot{\mathbf{V}}_R + \mathbb{K}\mathbf{V}_R = \mathbf{0} \quad (3)$$

Note that we have not presented the modeling of damping matrix \mathbb{B} in this paper. Models such as proportional damping, given by $\mathbb{B} = b_m \mathbb{M} + b_k \mathbb{K}$, are widely used in the literature [18], where b_m and b_k are constants that depend on material properties and are experimentally determined from sine-sweep frequency response measurements. For the design of active or passive damping in flexure mechanisms, a survey and foam-based methods are detailed in [19].

III. DYNAMIC PERFORMANCE OF DIAPHRAGM FLEXURES

In this section, we use the dynamic models developed from Section II-C to examine (i) modal coupling (ii) natural frequencies, and (iii) the performance trade-offs of diaphragm flexure mechanisms.

A. Coupling

Static and dynamic decoupling is desirable, for instance, when the diaphragm flexure mechanism is controlled to vertically position the central rigid mass while ensuring low error motions in the other DOFs, namely pitch and roll. Stable decoupled systems tend to be more amenable to low error motions even under open-loop control. It should, however, be noted that perfect decoupling cannot be achieved in practice owing to non-uniformities arising from manufacturing or material properties. Nonetheless, designing a compliant mechanism to be as close to a decoupled dynamic system as possible is desirable [20].

Based on the analysis presented in Section II-A, the conditions necessary for the off-diagonal terms in the global mass \mathbb{M} and stiffness \mathbb{K} matrices to be zero are as follows:

$$\sum_{i=1}^n \cos \alpha_i = 0; \quad \sum_{i=1}^n \sin \alpha_i = 0; \quad \sum_{i=1}^n \sin 2\alpha_i = 0; \quad (4)$$

Hence, the geometric arrangement of a number $n \geq 3$ of flexures around the central rigid mass allows for the overall mechanism to be close to being statically and dynamically decoupled if the above conditions are satisfied.

B. Natural Frequencies

The best -3 dB bandwidth possible for a closed-loop system depends on many factors, including the natural frequencies or poles of the open-loop plant. Fig. 3 shows the plots of undamped natural frequencies of the first three modes of the symmetric diaphragm flexure of Fig. 1. The plots show the variation corresponding to diaphragm flexure configurations with flexural beam length, ℓ , varied in the range of about 0.5 in to 3 in, while keeping the footprint $2\ell+2R$ at a constant value of 7 in. This constant footprint is chosen as a scaling factor for the length dimension and will be used in Section III-C to normalize all lengths in the design to formulate a non-dimensional study.

The plots of Fig. 1 show values of the undamped natural frequencies obtained from models based on St. Venant's torsion theory and one of two distinct beam bending theories—either (i) Timoshenko beam bending theory, or (ii) Euler Bernoulli beam bending theory. As explained earlier, the former beam bending theory accounts for shear and rotational effects versus, while the latter does not. In the plots of the figure, the frequency values obtained from a commercial FEA package are superimposed for comparison of the chosen models.

The trends observed for the variation of natural frequencies for small flexural beam lengths is as expected, since small beam lengths result in large stiffness. Since the footprint is maintained constant, smaller beam lengths also imply large radius of the central disk and hence larger moving mass. However, the cubic dependence of stiffness on beam length dominates over the square dependence of mass on radius of the disk; hence the large natural frequencies at short beam lengths. For large beam lengths, the radius of the central disk is small, and hence the moving mass.² This effect is marginally larger than the loss in stiffness and hence the slight increase in natural frequency at large beam lengths.

For flexural beam lengths smaller than the shear approximation length factor $c \approx 0.6$ in (i.e. smaller length to thickness aspect ratios), the Timoshenko model matches the trend from the FEA data better than the Euler-Bernoulli model. This confirms the prediction that shear effects dominate at beam lengths comparable to beam thickness and agrees with similar observations for short AFM cantilevers in [21].

Closed-form expressions for the natural frequency of the first three-dominant modes in the decoupled case, for large flexure lengths, are presented in Table I. These expressions can be used as part of formulating an optimization problem, or to gain useful insights from parametric dependencies in designing a precision angular alignment setup based on diaphragm flexures.

C. Performance Trade-offs

The design space for utilizing flexure-based precision angular alignment mechanisms can be characterizing in terms

²At the length scale of the diaphragm flexure discussed here, the moving mass is mainly composed of the central rigid disk. The lumped mass of the flexural beam is small at this length scale. However, it can be higher in other length scales, as in the case of a torsional MEMS mirror.

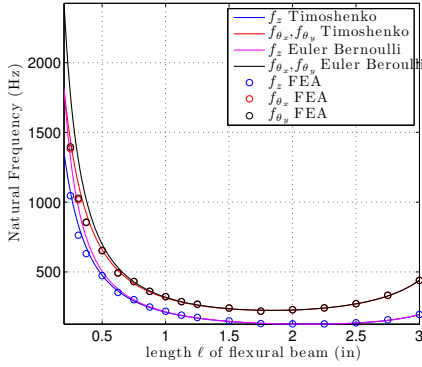


Fig. 3. Plot of undamped natural frequencies of first three modes of the diaphragm flexure of Fig. 1 for beam length ℓ varying from about 0.2 in to 3 in, keeping foot-print $D_0 = 2\ell + 2R$ at a constant value of 7 in. Other parameter values used are: beam width $W = 0.75$ in, beam thickness $H = 0.1$ in, central rigid disk thickness $T = 2.5$ in, poisson's ratio $\nu = 0.33$, elastic modulus $E = 69$ GPa, density $\rho = 2700 \frac{\text{kg}}{\text{m}^3}$.

TABLE I

CLOSED-FORM EXPRESSIONS FOR NATURAL FREQUENCIES OF FIRST THREE MODES OF DIAPHRAGM FLEXURE.

$$\omega_z = \sqrt{\frac{\frac{3EW^3H^3}{l^3}}{m + \frac{39}{32}m_f}}$$

$$\omega_{\theta_x, \theta_y} = \sqrt{\frac{\frac{3EW^3H^3}{l^3} (L^2 + 3R^2 + 3LR) + \frac{GW^3H^3}{2l^3}}{m(\frac{3R^2 + l^2}{12}) + m_f(\frac{l^2 + 39R^2 + 11LR}{70} + \frac{W^2 + H^2}{24})}}$$

of key parameters such as the range, payload capacity, and bandwidth. Fig. 4 shows the variation of the key non-dimensionalized performance parameters as a function of the non-dimensional flexural beam length ℓ for all diaphragm flexures with a constant footprint of $D = 2\ell + 2R$. The performance parameters plotted in the figure are (i) the natural frequencies of the first three modes, namely deflection z and the two rotations θ_x and θ_y , (ii) the maximum load-capacity, F_{max} , defined as the load that causes the resultant axial stress in the flexural beams to reach the yield strength, σ_y , of the material within a safety factor η , and (iii) the maximum vertical deflection δ_{max} , i.e. range under a given load. The normalization factors used for non-dimensionalizing the parameters are tabulated in Table II, where ρ and E are the density and elastic modulus, respectively, of the material constituting the diaphragm flexure.

The trade-off between load-capacity and range at different flexural beam lengths is evident from the figure. Small beam

TABLE II

NORMALIZATION FACTORS USED FOR DESIGN PARAMETERS IN FIG. 4.

Parameter	Normalization Factor
ℓ	$D = 2\ell + 2R$
$f_z, f_{\theta_x}, f_{\theta_y}$	$f_0 = \frac{1}{4\pi} \sqrt{\frac{E}{\rho D^2}}$
F_{max}	$F_0 = \frac{1}{6} \frac{WH^2}{D} \frac{100\sigma_y}{\eta}$
δ_{max}	$\delta_0 = \frac{10^6 F_0}{ED}$

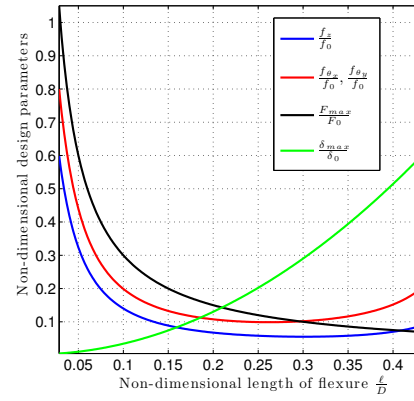


Fig. 4. Non-dimensional plots capturing the key dynamic performance parameters for diaphragm flexures of Fig. 3 with $n = 3$ flexural beams of the same footprint D , but different flexure lengths ranging in the approximate range 0-0.45 D . The parameters of interest are (i) the natural frequency of first three modes f_z , f_{θ_x} , and f_{θ_y} , all normalized by f_0 , (ii) load capacity F_{max} normalized by F_0 and (iii) static vertical range δ_{max} normalized by δ_0 .

lengths allow for large load capacity and low range, whereas large beam lengths allow for low load capacity and large range. Natural frequencies are relatively low for intermediate beam lengths. The trade-off between natural frequencies and range is evident for small beam lengths, since stiffer beams have smaller deflections. The compromise between natural frequency and range is relatively mild at large beam lengths.

IV. STATE-SPACE PERFORMANCE ANALYSIS

Characterization of parameters such as maximum displacement (or range), maximum velocity and acceleration is critical for precision motion control applications. A procedure for identifying the static ($\omega = 0$) values of these parameters is developed for precision control of ball-screw drives in [22]. In this section, we present a state-space approach for determining the design performance parameters — maximum values of deflection (or range), velocity, and acceleration that are possible not only for static ($\omega = 0$) but for a large range of operating frequencies.

We follow the approach for the case of a diaphragm flexure used for precision angle alignment. To account for the case when symmetry cannot be ensured for the diaphragm flexure, we assume a coupled multi-input multi-output (MIMO) model, as against a collection of independent single-input single-output (SISO) models. We focus our analyses to parameters such as maximum vertical and angular displacement (range), velocity, and acceleration. The presented approach can be extended to map other design parameters to the state-space. Further, while the ideas presented here are general and applicable to the case when state or output feedback control is used as well, we focus our analysis on just the open-loop system.

A. State Space Formulation

We begin with a state vector \mathbf{x} containing the generalized coordinates depicting the equations of motion of the system.

One choice of state variables could be the generalized displacements and their first-order derivatives.

$$\dot{\mathbf{x}}_{m \times 1} = \mathbf{A}_{m \times m} \mathbf{x}_{m \times 1} + \mathbf{B}_{m \times r} \mathbf{u}_{r \times 1} \quad (5)$$

$$\mathbf{y}_{p \times 1} = \mathbf{C}_{p \times m} \mathbf{x}_{m \times 1} + \mathbf{D}_{p \times r} \mathbf{u}_{r \times 1} \quad (6)$$

The goal here is to find the maximum values of displacements, velocities, and acceleration for any set of inputs (which can be oriented in any direction in the input space). That means we need to compute the upper bounds on the amplification of a scalar component x_i , which is derived as:

$$x_i = \mathbf{E}_{i1 \times m} \mathbf{x}_{m \times 1} \quad (7)$$

where the i^{th} element of the row vector \mathbf{E}_i is 1 and the rest of the $m - 1$ elements are zero. The component x_i can be any design variable, such as angular velocity, or vertical deflection of the diaphragm flexure.

For a chosen control law, in the Laplace domain, the following relations hold between the state vector $\mathbf{X}(s)_{m \times 1}$, its i^{th} component $X_i(s)$, and the input vector $\mathbf{U}(s)$:

$$\mathbf{X}(s)_{m \times 1} = \mathbf{G}(s)_{m \times r} \mathbf{U}(s)_{r \times 1} \quad (8)$$

$$X_i(s)_{1 \times 1} = \mathbf{E}_{i1 \times m} \mathbf{G}(s)_{m \times r} \mathbf{U}(s)_{r \times 1} \quad (9)$$

The maximum amplification of the component $X_i(s)$ for a given input $\mathbf{U}(s)$ can be expressed as the 2-induced (Euclidean) norm of the gain matrix $\mathbf{E}_{i1 \times m} \mathbf{G}(s)_{m \times r}$. For the choice of \mathbf{E}_i , the gain matrix reduces to the i^{th} row of $\mathbf{G}(s)$. Hence, its 2-induced norm reduces to a vector norm, and is given by its lone singular value. This singular value of $\mathbf{E}_{i1 \times m} \mathbf{G}(s)_{m \times r}$ is always smaller than or equal to the singular values of the matrix $\mathbf{G}(s)$ and hence provides a tighter bound on the amplification of $X_i(s)$.

B. Application to Diaphragm Flexure

We now apply the above formulation to the case of the diaphragm flexure of Fig. 3 to derive tight upper bounds³ on the amplification of state vector components, such as vertical deflection, or say, maximum angular velocity of the diaphragm flexure in a given control situation. We do not consider the feedback control problem here; however, the proposed method can be extended to that case as well.

With the choice of \mathbf{E}_i as described earlier, the maximum bound on each of the components of the state vector are found as shown in Fig. 5 for the diaphragm flexure of Fig. 3 containing three flexural beam units arranged symmetrically around the central rigid mass, and with linear actuators located at angles: $0, \frac{2\pi}{3}, \frac{4\pi}{3}$. The system is decoupled as seen from the variation of the singular values. With zero damping at the resonance peak, the maximum values of all variables assume exceedingly large values at the resonance frequency.

³The lower bound is zero, since for zero inputs, the components of the state vector are all zero.

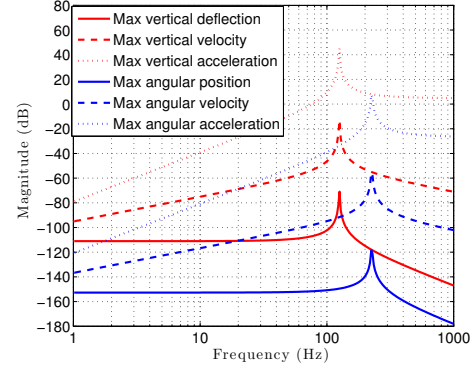


Fig. 5. The maximum amplification of states for an unit input vector (along any direction in the position space) is plotted for the case of three flexural beam units arranged symmetrically around the central rigid mass.

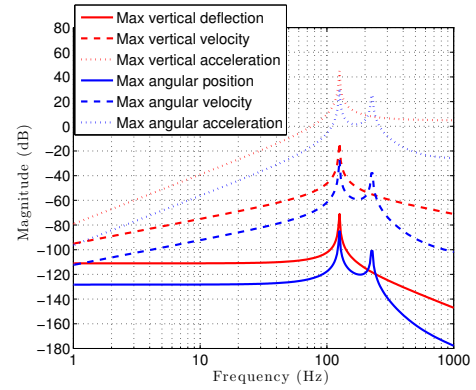


Fig. 6. The maximum amplification of states for an unit input vector (along any direction in the position space) is plotted for the case when a 1° misalignment of one of the flexural beam units is caused by a manufacturing error. Note that the system is now coupled as seen from the variation of the singular values.

C. Effect of Deviation from Symmetry

The same analysis is repeated for the case when a 1° misalignment of one of the flexural beam units is caused by a manufacturing error. The system is now coupled, with deflection and angular position being dependent on each other, as seen from the two resonance peaks appearing in the variation of the singular values in Fig. 6. This coupling implies that the angular position can assume exceedingly large values at a resonance frequency lower than that expected when perfect symmetry is ensured. The input directions that correspond to the maximum bound on a component $X_i(j\omega)$ at a chosen frequency ω lie along the right eigen vectors of the matrix $\mathbf{G}_i^H(j\omega) \mathbf{G}_i(j\omega)$, where $\mathbf{G}_i(j\omega)$ is the i^{th} row of the matrix $\mathbf{G}(j\omega)$.

In summary, the benefits of using this approach for specifying the design performance variables are two fold — (i) it is applicable in case of deviations from perfect symmetry, allowing to analyze the effects of the deviations, and (ii) it gives the bounds not only for the static case ($\omega = 0$) but also for the desired frequency range of interest. This approach can be incorporated into the design decision-

making process, along with other important considerations, such as constraints imposed by physical limits, for example, saturation of the actuators, or limit stops in the path of a motion stage.

V. CONCLUSIONS

In this paper, we have examined the need for diaphragm flexures in precision angular positioning applications. To accurately characterize the dynamics, we assembled lumped parameter models for individual flexural building blocks and the overall mechanism. Models included here can capture shear effects that dominate for flexures with comparable thickness and length. We identified the key performance trade-offs in range, load-capacity, and natural frequencies of the diaphragm flexure. Further, a state-space performance analysis was formulated to capture the maximum values of performance specifications such as linear or angular position. We plan to test the presented models through system identification experiments in future. While the tested models will be useful for control implementations, they can also be a valuable tool for identifying trade-offs in design synthesis.

ACKNOWLEDGEMENTS

This work was supported by funding grants from the Manufacturing Systems and Technology program under the Singapore MIT Alliance. We are grateful to Prof. Harry Asada, Prof. Martin L. Culpepper, and the anonymous reviewers for their comments and suggestions. The first author would also like to thank Ajay A. Deshpande and Mythili R. Vutukuru for their discussions on parts of the analysis.

APPENDIX

Distributed Parameter Model and Approximation

The set of partial differential equations governing Timoshenko beam bending and St. Venant's torsion under the assumptions stated in Section II-A can be written in terms of the deflection $w(x,t)$, slope $\theta(x,t)$, and angle of twist $\phi(x,t)$ as follows [17]:

$$EI_{yy} \frac{\partial^2 \theta(x,t)}{\partial x^2} + \kappa AG \left\{ \frac{\partial w(x,t)}{\partial x} - \theta(x,t) \right\} - \rho I_{yy} \frac{\partial^2 \theta(x,t)}{\partial t^2} = 0 \quad (10)$$

$$\rho A \frac{\partial^2 w(x,t)}{\partial x^2} - \kappa AG \left\{ \frac{\partial^2 w(x,t)}{\partial x^2} - \frac{\partial \theta(x,t)}{\partial x} \right\} = 0 \quad (11)$$

$$GJ_{xx} \frac{\partial^2 \phi(x,t)}{\partial x^2} + I_{xx} \frac{\partial^2 \phi(x,t)}{\partial t^2} = 0 \quad (12)$$

where ρ, E, GJ_{xx} are the density, elastic modulus, and torsional rigidity, respectively; A, I_{yy} , and κ are the cross-sectional area, area moment of inertia about the neutral axis Y, and a geometry-dependent shear-factor, respectively. For a rectangular cross-section κ assumes a value of 0.833 [21]. The component values of the mass \mathbb{M} and stiffness \mathbb{K} matrices are listed in Tables III and IV. The parameters used in the tables are $\alpha = \left\{ \frac{1}{1+2p} \right\}^2$ and $\beta = \frac{EI_{yy}}{6} \frac{c^2}{\ell^3}$, where, $p = (\frac{\ell}{t})^2$, and $c = \sqrt{\frac{6EI_{yy}}{\kappa AG}}$ representing the length scale at which effects of shear dominate. For a flexural beam with rectangular cross-section of height H , c reduces to $\sqrt{1.1(1+\nu)H}$, where ν is the poisson's ratio of the material.

REFERENCES

- [1] Loney GC, "High bandwidth steering mirror," US Patent 5,110,195, 1992.
- [2] Choi BJ, Sreenivasan SV, Johnson S, et al, "Design of orientation stages for step and flash imprint lithography," Precision Engineering Journal, vol. 25 (3), pp 192-199, July 2001.
- [3] Choi KB, Lee JJ "Passive compliant wafer stage for single-step nano-imprint lithography," Review of Scientific Instruments, 76 (7): Art. No. 075106 Jul 2005.
- [4] Kendale AM, "Automation of soft lithographic microcontact printing," SM thesis, Department of Mechanical Engineering, Massachusetts Institute of Technology, Cambridge MA, 2002.

TABLE III
MASS MATRIX COMPONENT VALUES

M_1	$= \alpha m_f \left[\frac{13}{35} + \frac{7}{5} \left(\frac{\ell}{t} \right)^2 + \frac{4}{3} \left(\frac{\ell}{t} \right)^4 \right] + \frac{6}{5} \frac{\rho \alpha I_{yy}}{\ell}$
M_2	$= -\alpha m_f \ell \left[\frac{11}{210} + \frac{11}{60} \left(\frac{\ell}{t} \right)^2 + \frac{1}{6} \left(\frac{\ell}{t} \right)^4 \right] + \rho \alpha I_{yy} \left[\frac{1}{10} + \left(\frac{\ell}{t} \right)^2 \right]$
M_3	$= \alpha m_f \ell^2 \left[\frac{1}{105} + \frac{1}{30} \left\{ \left(\frac{\ell}{t} \right)^2 + \left(\frac{\ell}{t} \right)^4 \right\} \right] + \rho \alpha I_{yy} \ell \left[\frac{2}{15} + \frac{1}{3} \left(\frac{\ell}{t} \right)^2 + \frac{4}{3} \left(\frac{\ell}{t} \right)^4 \right]$
M_4	$= \frac{I_{xx}}{3}$

TABLE IV
STIFFNESS MATRIX COMPONENT VALUES

K_1	$= \alpha \frac{12EI}{\ell^3} + 144\alpha\beta$
K_2	$= -\alpha \frac{6EI}{\ell^2} - 72\alpha\beta$
K_3	$= \alpha \frac{4EI}{\ell} \left[1 + \left(\frac{\ell}{t} \right)^2 + \left(\frac{\ell}{t} \right)^4 \right] + 36\alpha\beta$
K_4	$= \frac{GJ_{xx}}{\ell}$

- [5] Chan HB, Aksyuk VA, Kleiman RN, et al, "Quantum mechanical actuation of microelectromechanical systems by the Casimir force," Science, vol. 291 (5510): 1941-1944, Mar 2001; V. Shilpiekandula, "Progress through Mechanics: Small-scale Gaps," *Mechanics* (Publication of the American Academy of Mechanics), vol. 35, no. 9-10, pp. 3-6, Sep-Oct 2006.
- [6] Slocum AH, "Precision machine design," Englewood Cliffs, NJ, Prentice Hall, 1992; Smith ST, "Flexures: elements of elastic mechanisms," Amsterdam, Gordon and Breach, 2000.
- [7] Awtar S, Slocum AH, Sevincer E. "Characteristics of beam-based flexure modules," Journal of Mechanical Design, vol. 129 (6): 625-639 Jun 2007.
- [8] V. Shilpiekandula and K. Youcef-Toumi, "Modeling and Control of a Programmable Filter for Separation of Biologically Active Molecules," In Proceedings of *American Control Conference*, pp. 394-399, June 2005; Awtar S and Slocum AH, "Design of Flexure Stages based on a Symmetric Diaphragm Flexure," In Proceedings of American Society for Precision Engineering Annual Meeting, no. 1803, Norfolk, VA, 2005.
- [9] Lobontiu N, "Compliant mechanisms : design of flexure hinges," Boca Raton, CRC Press, 2003; Howell LL, "Compliant mechanisms," New York , Wiley 2001.
- [10] Jones RV, "Instruments and Experiences: Papers on Measurement and Instrument Design," John Wiley, 1988; Hopkins JB, "Design of Parallel Flexure Systems via Freedom and Constraint Topologies," Master of Science Thesis, Massachusetts Institute of Technology, 2005.
- [11] Li Z, and S. Kota, "Dynamic Analysis of Compliant Mechanisms," "Proceedings of IDETC, 27th Biannual Mechanisms and Robotics Conference," Sep 29 - Oct 2, Montreal, Canada, 2002.
- [12] Choi KB, "Dynamics of a compliant mechanism based on flexure hinges," Proceedings of the Institution of Mechanical Engineers, Part-C, Journal of Mechanical Engineering Science 219 (2): 225-235 Feb 2005.
- [13] Choi KB, Han CS, "Optimal design of a compliant mechanism with circular notch flexure hinges," Proceedings of the institution of Mechanical Engineers, Part-C, Journal of Mechanical Engineering Science 221 (3): 385-392 Mar 2007.
- [14] Weaver W, Timoshenko SP, Young DH, "Vibration problems in engineering," New York, Wiley, 1990.
- [15] Meirovitch L, "Computational Methods in Structural Dynamics," Sijthoff Noordhoff, Rockville MD, 1980.
- [16] Dwivedy SK, Eberhard P. "Dynamic analysis of flexible manipulators, a literature review," Mechanism and Machine Theory, vol. 41 (7): 749-777, July 2006.
- [17] Przemieniecki JS, "Theory of matrix structural analysis," New York, McGraw-Hill, 1968; Ganesan N and Engels RC, "A dynamic finite element model for the Timoshenko beam," AIAA-1990-3547 Space Programs and Technologies Conference, Huntsville AL, Sep 1990.
- [18] Inman DJ, "Engineering vibration," Englewood Cliffs, NJ, Prentice Hall, 1994.
- [19] Varanasi KK and Nayfeh SA, "Damping of Flexural Vibration Using Low-Density, Low-Wave-Speed Media," Journal of Sound and Vibration, vol. 292, pp. 402-414, 2006.
- [20] Deo HV, Suh NP, "Mathematical transforms in design: Case study on feedback control of a customizable automotive suspension," CIRP Annals — Manufacturing Technology, vol. 53 (1), pp. 125-128, 2004.
- [21] Hsu JC, Lee HL, Chang WJ, "Flexural vibration frequency of atomic force microscope cantilevers using the Timoshenko beam model," Nanotechnology, vol.18 (28): Art. No. 285503, July 2007.
- [22] Varanasi KK, Nayfeh SA, "The Dynamics of Lead-Screw Drives: Low-Order Modeling and Experiments," Journal of Dynamic Systems, Measurement, and Control, Transactions of the ASME, vol. 126, pp. 388-396, 2004.